43rd AIAA/ASME/SAE/ASEE Joint Propulsion Conference & Exhibit
8 - 11 July 2007, Cincinnati, OH

AIAA 2007-5207

Design and Construction of an Electron Trap for Studying Cross-Field Mobility in Hall Thrusters

Emily C. Fossum* and Lyon B. King†
Michigan Technological University, Houghton, MI, 49931, U.S.A

Excessive cross-field electron mobility in Hall thrusters has a negative effect on thruster efficiency and has been shown experimentally to be much larger than predicted by classical collisional transport theory. An electron trapping apparatus was constructed at Michigan Tech's Isp Lab in order to study electron dynamics in the defining electric and magnetic fields of a Hall-effect thruster. This apparatus was designed to stably trap a non-neutral electron plasma in a confining volume in order to study these dynamics in a highly controlled environment. Electrons are confined using only electric and magnetic fields in the absence of ions and dielectric walls, which are present in a typical Hall thruster. Mobility studies on a low-density, non-neutral plasma provide several advantages over a typical Hall thuster's quasi-neutral plasma, including a well-defined electric field and the ability to take internal electrostatic probe measurements in the "acceleration" region. Cross-field electron mobility was investigated in response to magnetic and electric field strengths and background neutral density. Experimental design considerations including loading mechanisms, trapping potential, magnetic field design, calibration, and diagnostic techniques are presented along with preliminary experimental results. In this investigation, measured cross-field mobility is much larger than classical theory predicts and appears to be consistent with Bohm-like mobility rather than classical mobility.

Nomenclature

B_r	=	radial magnetic field
$\mathbf{B}$	=	magnetic field vector
B	=	magnitude of **B**
$\hat{b}$	=	unit vector in the **B**-field direction
$\mathbf{c}$	=	thermal velocity
ε_0	=	permittivity of free space
e	=	elementary charge
$\mathbf{E}$	=	electric field vector
E_z	=	axial electric field
$\mathbf{F}_\mu$	=	magnetic mirror force
$\mathbf{F}_{E\|\|}$	=	parallel electric field force
$\mathbf{F}_C$	=	centrifugal force
Φ	=	electric potential
Φ_{eff}	=	effective trap potential
ϕ_p	=	plasma potential
J_a	=	current density at the anode
J_{ez}	=	cross-field electron current density
J_p	=	current density at the probe
m_e	=	electron mass
μ, μ_0	=	magnetic moment of gyrating particle
μ_{ez}	=	cross-field electron mobility
n_e, n_∞	=	electron number density
n_0	=	neutral particle density

* GRA, Mechanical Engineering, ecfossum@mtu.edu
† Associate Professor, Mechanical Engineering, lbking@mtu.edu

ν_m = momentum-transfer collision frequency for electrons
q = particle charge
r_L = electron Larmor radius
σ = collision cross section
$\mathbf{u}$ = directed flow velocity
$u_{e\theta}$ = azimuthal electron velocity
u_{ez} = cross-field electron velocity
$u_{\perp}$ = electron perpendicular velocity
V_{ac} = anode-to-cathode voltage
V_p = probe voltage
$\bar{v}_e$ = average thermal velocity of electrons
v_f = flow velocity
v_{th} = thermal velocity
ω_{ce} = electron cyclotron frequency
Ω_H = electron Hall parameter

I. Introduction

HALL thrusters are highly efficient in-space propulsion devices used mainly for satellite station keeping and orbit correcting. The defining characteristic of Hall thrusters is the crossed axial electric and radial magnetic fields. The electric field accelerates ionized gas from the thruster, which produces thrust, whereas the radial magnetic field sustains the electric field by impeding the highly mobile electron flow to the anode. The criteria of the E- and B-fields are such that the electron gyro radius is small compared with apparatus dimensions while the gyro radius and mean free path for ions are larger than apparatus dimensions; these criteria are necessary so that ions are only affected by the electric field, where the electron trajectories are controlled by both electric and magnetic fields. The crossed E and B fields induce the confining ExB electron drift, or Hall current, which holds electrons in azimuthal orbits around the discharge channel annulus.

Within the classical theory of electron mobility, collisions provide the only mechanism for motion across B-field lines, through electron-neutral or electron-wall collisions, with a step length per-collision on the order of the Larmor radius. A detailed description of how this dependence comes about can be found in Chen[1]. Cross-field mobility is defined as the constant of proportionality between the cross-field velocity of electrons, u_{ez}, and the axial electric field, E_z:

$$\mu_{ez} \equiv \frac{u_{ez}}{E_z}. \tag{1}$$

Classically the mobility of electrons is given by

$$\mu_{ez} = \frac{e}{m_e \nu_m} \frac{1}{1 + \omega_{ce}^2 / \nu_m^2} \tag{2}$$

where ω_{ce} is the electron cyclotron frequency and ν_m is the momentum-transfer collision frequency for electrons. The analysis of mobility presented here is based on the assumption of a large Hall parameter, Ω_H, that is $\Omega_H = \omega_{ce}/\nu_m >> 1$, a case that is required for Hall thruster operation. (In the case that $\omega_{ce}/\nu_m << 1$ magnetic field would have little effect on cross-field mobility, as electrons would have many collisions in a single gyration and would quickly eliminate the electric field necessary to produce thrust.) Given the case of a large Hall parameter, the cross-field electron mobility in radial magnetic and axial electric fields becomes:

$$\mu_{ez} = \frac{\nu_m}{B_r \omega_{ce}}. \tag{3}$$

Classical mobility can therefore be determined at any point in the discharge channel where the magnetic field is known and an effective collision frequency can be estimated accurately.

In this way, electrons move across the radial B-field lines, gaining energy from the E-field and dissipating this energy through wall collisions and electron-neutral collisions, which ionize propellant neutrals. Cross-field electron transport is obviously necessary to sustain thruster discharge through ionizing collisions; however, electron current to the anode contributes to the total discharge current (and, hence, power) of the thruster but contributes no thrust, which corresponds to a decreased thruster efficiency.

In past experiments, the cross-field electron mobility has been found to be much larger than the classical collisional mobility model. The anomalous electron mobility was first observed in Hall thruster fields by Janes and Lowder[2] and later supported by Meezan, Hargus and Cappelli[3], who observed mobility up to 1,000 times greater than predicted by classical theory. Janes and Lowder predicted this departure to be caused in part by azimuthal variations in plasma density, and thus electric field, creating a secondary drift term in the axial direction. Plasma fluctuations have since been characterized and are now well-documented[4,5,6] leading to Meezan's work supporting Janes and Lowder's initial hypothesis. Meezan provided the first quantified measure of mobility as it varies with axial position in the discharge channel, finding the greatest departure from the classical model at the location where plasma fluctuations were shown to exist. Others have hypothesized that the dielectric wall interactions play a significant role in electron transport and attempts have been made to quantify and model the near wall region of the discharge channel[7,8].

The approach used in this investigation removes ion fluctuations and wall interactions by examining the electron dynamics of a low-density, pure electron plasma in a Hall thruster's defining fields with an independently controlled electric field in vacuum. While such an approach has not been documented in Hall thruster investigations, studies of non-neutral plasmas have proven to be useful for numerous types of charged particle transport experiments[9,10,11,12,13,14]. Without ion effects or wall-interactions, mobility in such Hall thruster fields is studied in its purest sense and a comparison between classical and experimentally determined mobility can be made. The focus of this paper is to present an analysis of the trap apparatus including the stability of the electron plasma, magnetic and electric field optimizations, and probe characteristics, along with preliminary results.

II. Description of Apparatus

A. Electron Trap

An electron trapping apparatus shown in Fig. 1 was constructed with a "confining volume" that reproduces the defining characteristics of a Hall thruster's accelerating region, referred to as the confining region. The physical size of the trap is about four times the size of a typical flight-scale Hall thruster in order to operate over a greater range of magnetic fields while maintaining scaling parameters, most importantly $r_L << L$ where r_L is the electron Larmor radius and L is a characteristic length of the trap. A larger trap also allows ease of probe access of the confining region. A radial magnetic field was created with a shape and strength that is similar to that of a Hall thruster through use of magnetic windings on inner and outer magnetic poles. An axial electric field was created via parallel plate electrodes in vacuum. Carefully shaped electrodes were employed to ensure that electric equipotentials coincided with magnetic field lines within the trap volume, which is similar to the quasi-neutral plasma potential structure found in a Hall thruster.

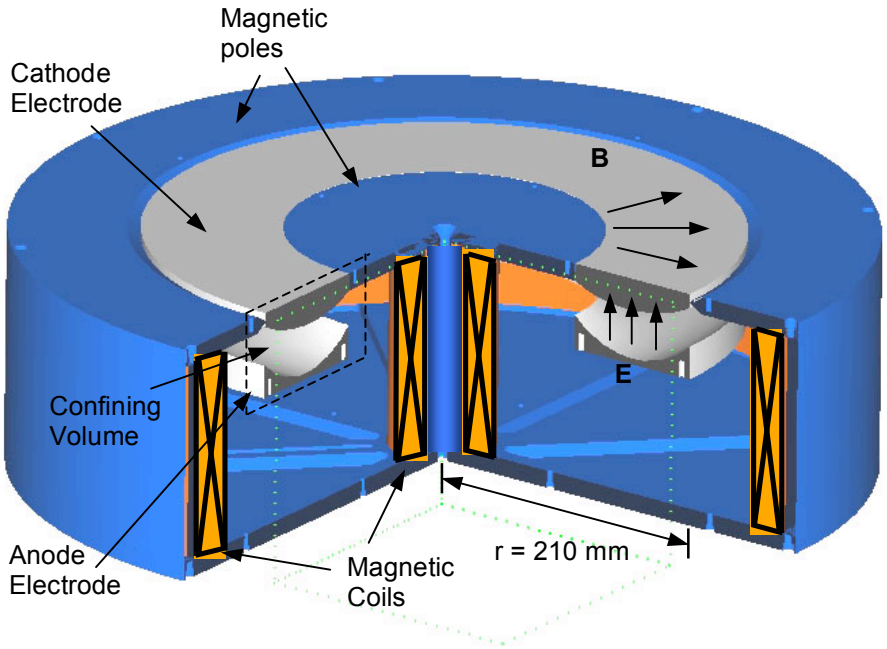

Figure 1. Electron trapping apparatus

The trap is operated in the Isp Lab's Vacuum Test Facility #2, a 2-m-diameter, 4-m-long cylindrical vacuum chamber. Rough pumping is accomplished through a two-stage mechanical pump, capable of 400 cfm. High vacuum is achieved through the use of three turbomolecular pumps with a combined throughput of 6,000 liters per second providing a base pressure below 10^{-6} Torr. An ion gage is mounted directly to the electron trap in order to obtain a local measure of pressure inside the trapping volume. Krypton gas was introduced to vary the base pressure from 10^{-6} to 10^{-4} Torr.

B. Trap Loading

Electrons are injected into the trap using a thermionically emitting thoriated tungsten filament placed entirely inside the trap at the cathode. A filament heater circuit was isolated with an isolation transformer and biased negatively with respect to ground. In order to emit low energy electrons the filament bias was increased until no emission current was observed and then tuned about 100-500 mV below this potential. Since the filament is entirely within the confining volume the emission current equals the loss rate of electrons from the confining volume, either by radial losses or by axial mobility, which can be measured by current collected at the anode. The trap density can be controlled by varying the emission characteristics of the filament.

C. Diagnostics

A number of plasma parameters can be determined through current measurements at the anode and on an electrostatic probe. The axial electron current was measured at the anode through a low-impedance, low-noise current amplifier. An internal planar Langmuir probe is used to obtain plasma parameters such as electron temperature and electron density. For this in-situ measurement, a 2.36-mm-diameter probe is positioned 180 degrees from the emission filament so that the planar collection surface is sensitive only to azimuthal electron current. The probe is positioned at the center of the channel annulus (r=160 mm) and 10 mm from the anode (z=-45 mm). The probe is encased in an alumina sheath where the exposed collection area of the probe is aligned orthogonally to the azimuthal Hall current. For typical field configurations investigated with this trap, namely Br~50 G to 200 G and Ez~$1x10^3$ V/m to $1x10^4$ V/m, an electron cloud with density ~10^{10} m^{-3} would create a probe current on the order of tens of nano-Amps, which can be easily measured by a Keithley sourcemeter.

III. Design Considerations

A. Field Considerations

In a typical Hall thruster with a quasi-neutral plasma, the plasma potential structure has been found to coincide with magnetic field lines[15] such that electrons are thermally mobile along field lines. The challenge in creating the electric and magnetic fields for the electron trap was meeting the criterion that magnetic field lines and lines of constant electric potential coincide in vacuum. The magnetic field was modeled to replicate the acceleration region of a Hall thruster. A magnetic field solver, Maxwell[16], was used in order to map the field lines, and physical electrodes were constructed such that the electrode surfaces were coincident with local magnetic field lines. The vacuum electric field induced by the electrodes was taken to be rigid during trap operation as the contribution to the field from a low density plasma is negligible (as is described in Section III.B., Eq. 4). Figure 4 shows the contoured electrodes and the magnetic field lines superimposed on the electric equipotential lines. This agreement in the field lines over the majority of the confining volume indicates that electrons would be thermally mobile along field lines and their guiding center paths would be parallel to the electrode contours. At the inner and outer radii of the confinement volume the electric equipotential lines depart from the magnetic field lines providing a parallel electric force that is radially confining for electrons at the volume periphery.

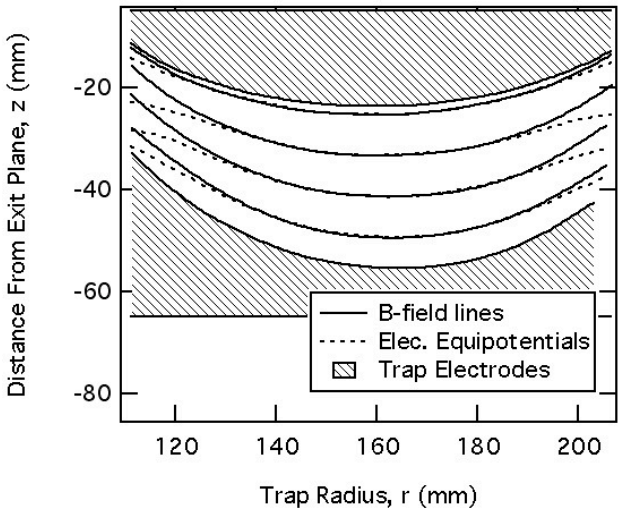

Figure 2. Magnetic and Electric Equipotential Lines.

B. Stability Analysis

Electrons are confined axially on closed annular magnetic surfaces due to the radial magnetic field, and thus a stability analysis was conducted along field lines to ensure radial stability. In a non-neutral plasma, a space charge exists from the mutual repulsion of the electrons due to the absence of shielding ions. The negative space charge will induce a self-field that will locally depress the electric potential and drive the electrons to the walls of the trap; however, the magnitude of the space-charge field can be made negligible by adjusting the electron density within the trap.

The magnitude of the induced negative space charge is found from a solution of the Poisson equation, where Φ is the electric potential. Since the experiments presented here are sensitive primarily to the radial space-charge field (the axial space-charge field is much less than the applied E-field and is a negligible perturbation), the experimental geometry is approximated as a cylindrical annulus infinite in the z-dimension with inner radius r_{in} and outer radius rout. If the space between the cylinders is filled uniformly with electrons at density n_e=const., then the solution to the Poisson equation for the space-charge potential relative to the local potential of the trap becomes

$$\frac{\Phi(r)}{n_e} = \frac{e}{4\varepsilon_0}\left[r_{out}^2 - r^2 + \left(r_{out}^2 - r_{in}^2\right)\frac{\ln\left(r_{out}/r\right)}{\ln\left(r_{in}/r_{out}\right)}\right]. \tag{4}$$

The maximum potential occurs midway between r_{in} and r_{out} where, for the physical scale of the apparatus used in the present investigation, is $\Phi_{max}/n_e \sim 1\text{x}10_{-11}$ V-m^3. Thus, if the electron density were limited to $n_e < 10^{10}$ m^{-3} (very typical for electron non-neutral particle traps[10]), then the space-charge potential at chamber mid-radius would be on the order of 100 mV below unperturbed local trap potential. The moderate radial electric field induced by this 100 mV difference will not significantly alter the electron trajectories from those determined by the vacuum potential distribution alone as will be seen in the following single particle trajectory analysis. During the course of experiments electron density was monitored using the planar Langmuir probe and the emission characteristics of the tungsten injection filament were controlled to keep the electron density low enough to avoid significant space charge perturbation to the rigid fields.

The forces acting on an electron parallel to the magnetic field lines are the magnetic mirror force, $\mathbf{F}_\mu$, due to the B-field gradient, the parallel electric field force, $\mathbf{F}_{E\|}$, due to deviation between electric equipotentials and magnetic field lines at the trap edges, and the centrifugal force, $\mathbf{F}_C$, due to the azimuthal drift velocity of electrons. The total of these forces along a magnetic field line is given by:

$$F_{net} = -\mu\nabla(\mathbf{B}\bullet\hat{b}) + q\mathbf{E}\bullet\hat{b} + \frac{m_e u_{e\theta}{}^2\hat{r}}{r}\bullet\hat{b} \tag{5}$$

where $\hat{b}$ is the unit vector in the direction of the magnetic field vector given by $\hat{b} = \frac{\mathbf{B}}{B}$ and μ is the magnetic moment given by:

$$\mu = \frac{mu_{\perp}^{2}}{2B} \equiv \mu_0 = const. \tag{6}$$

Since we know the electric and magnetic fields at every point in the region of interest and can estimate a value for $u_{\perp}$ for the determination of μ_0, these equations can be numerically integrated in order to find an effective trap potential, Φ_{eff}, along a field line of interest.

The calculated forces along a representative field line are plotted in Fig. 3.a.-c. for the case of B_r~100 G and E_z~3x10^3 V/m, corresponding to an anode-to-cathode voltage, V_{ac}, of 100 V. For this electric field a typical electron temperature has been found to be on the order of 25 eV which corresponds to a $u_{\perp}$ of 3x10^6 m/s used in the calculation of the magnetic mirror force. The centrifugal force is much smaller than the confining forces of the parallel electric and magnetic mirror forces. It can be seen that the parallel electric force is small over the majority of the confinement space indicating good agreement between electric equipotentials and magnetic field lines, with a confining force only at the inner and outer radii of the trap. It is also notable that the magnetic mirror force is the dominant force near the inner radius of the confinement volume because the magnetic field experiences axial and radial divergence. However the magnetic mirror force is weaker at the outer radius because, although the field lines are converging axially, they are diverging radially as 1/r, and effect not apparent in Fig. 2. Thus, the parallel electric field force is on the same order of the magnetic mirror force near the outer radius of the trap and contributes to the radial confinement of electrons. The numerical integration of the net force gives effective trap potential, which is shown in Fig. 4. Three curves are plotted in Fig. 4, the solid line representing an electron with a velocity of 3x10^6, the two dashed curves representing upper and lower bounds that would include 90 percent of all electron velocities present assuming a Maxwellian distribution at an electron temperature of T_e=25 eV.

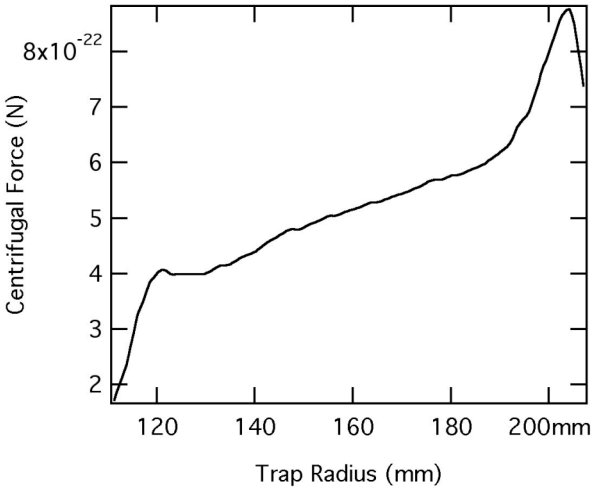

a.)

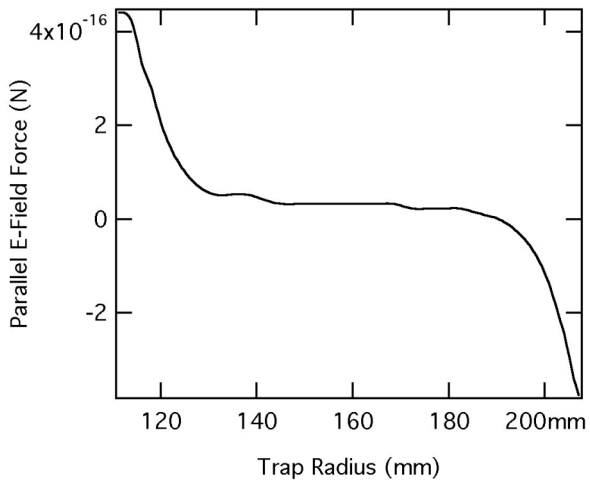

b.)

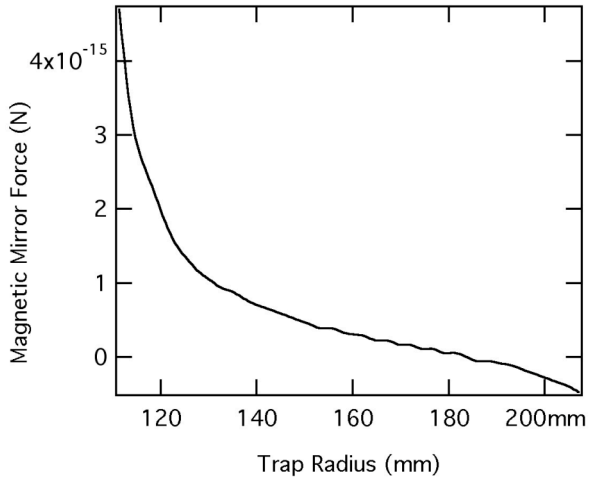

c.)

Figure 3. Forces acting on an electron within the trap volume.

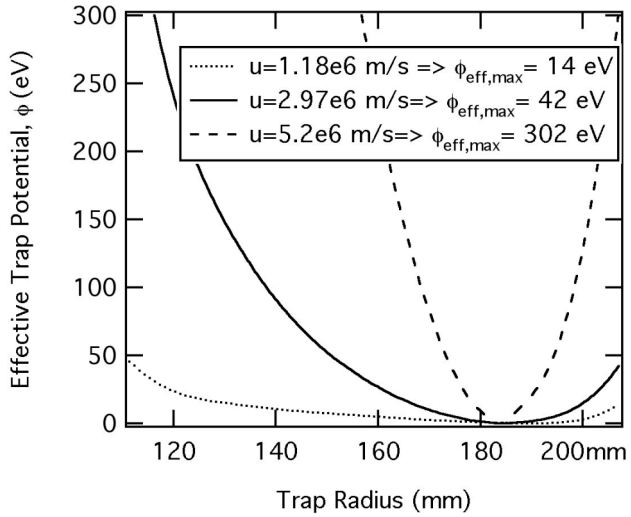

Figure 4. Effective trap potential for a magnetic field of 150 G and electric field of $4x10^3$ V/m.

C. Magnetic Field Calibration

The magnetic field and electric equipotential lines coincide for the case in the design example cited in Section III.A. where the inner and outer windings were at 1240 Amp-turns and 620 Amp-turns respectively, resulting in a magnetic field strength of 100 G at the channel centerline. However, in exploring electron mobility it is necessary to vary the strength of the magnetic field. Simply increasing or decreasing the inner and outer coil currents proportionally results in magnetic field geometries that are not necessarily aligned with the electric equipotentials. For example, Fig. 5 shows a Maxwell simulation of the field lines with an inner to outer Amp-turn ratio of 2:1, the same as the previous example, but with inner and outer windings of 3100 Amp-turns and 1550 Amp-turns, respectively resulting in a channel centerline magnetic field strength of 153 G. The departure of the magnetic field lines from the electric equipotential lines and electrode surface contours is apparent in Fig. 5, where Fig. 2 (in Section III.A.) shows proper tuning. To ensure alignment, the current ratio between the inner and outer magnetic coils needs to be tuned such that the lines coincide for all field strengths. Magnetic field simulations were conducted in order to determine the properly tuned current ratios for magnetic field strengths ranging from 80 to 200 G.

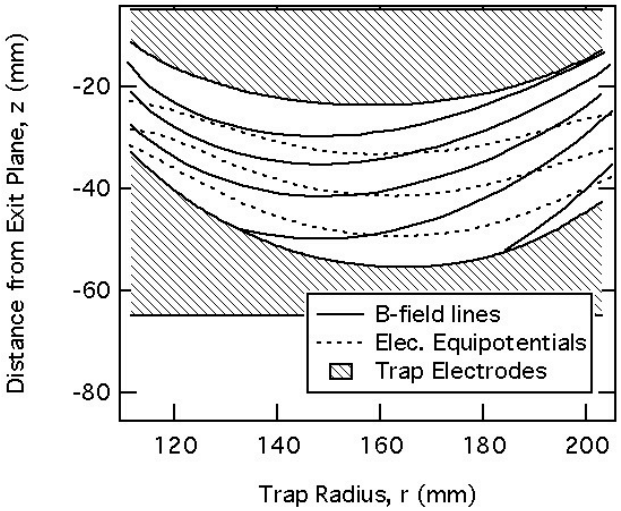

Figure 5. Magnetic and electric equipotential lines with improper magnetic field tuning.

It is assumed that the trap is most effective when the magnetic field lines coincide with the electric equipotential lines. Thus, the simulated optimal magnetic field conditions were experimentally validated by investigating trap effectiveness versus the outer coil Amp-turns while inner magnet current is held constant for each case, for a range of magnetic field strengths. The trap effectiveness was determined by monitoring the electron density as indicated by the current collected on a planar Langmuir probe biased to local potential and oriented to detect azimuthal flux. Figure 6 shows a sample plot of probe current versus the magnetic current ratio for the case of 5A, 3100 Amp-turns on the inner magnetic coils. The maximum probe current occurs at the optimal outer magnet current of 950 Amp-turns for 3100 Amp-turns on the inner coils. Similar probe investigations of trap performance were repeated over the range of inner coil currents considered in this work, where the optimal outer coil current was taken to be the value where the probe current was maximum. Figure 7 shows the optimal outer magnetic current that corresponds to each inner magnetic current for both the numerical simulations with Maxwell and experimental investigations using the probe technique. The results and agreement between these confirms the initial assumption of trap effectiveness and shows that the alignment of the field lines with electric equipotential lines is critical in the functionality of the trap, as probe current, and hence, trap density, is significantly affected by the magnetic field tuning.

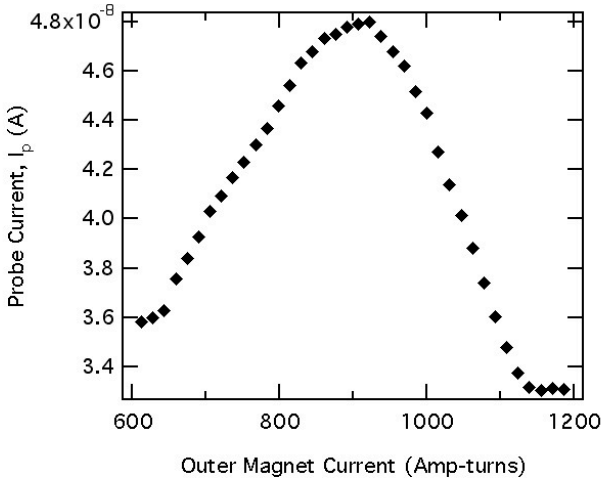

Figure 6. Optimization of magnet current ratio between inner and outer magnetic windings. The inner magnetic current was fixed at 3100 Amp-turns.

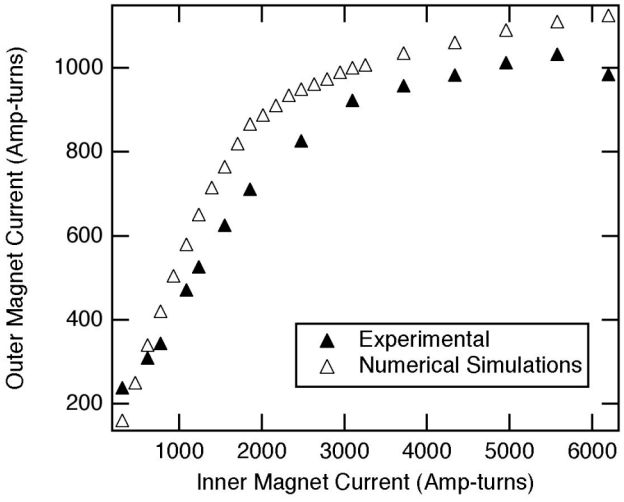

Figure 7. Optimal outer magnet current for each inner magnet current.

IV. Experimental Diagnostics

A. Probe Theory in Electron Plasmas

A planar Langmuir probe was used to diagnose the pure electron plasma. Because the non-neutral plasma has a directed azimuthal flow from the ExB drift, considerations must be made that deviate from probe theory in quasi-neutral plasmas with only thermal motion. Furthermore, in quasi-neutral plasmas density is found from the ion saturation current of an I-V probe characteristic, however, because ions are absent we are unable to interpret the I-V characteristic in this way. In our configuration the electron density and temperature can be found by examining the retarding region of the I-V characteristic (i.e. $V_p<\phi_p$, where V_p and ϕ_p are probe and plasma potential, respectively)[17,18]. A probe theory for the plasma conditions and geometry encountered in this work can be constructed by adapting the analyses of Gombosi for one-directional flux of a thermal gas on a moving surface[19]. In a flowing plasma the total velocity, **v**, is characterized by a combination of the random thermal motion, **c**, and the bulk motion of the plasma, or flow velocity, relative to the probe surface, **u,** where **v**=**u**+**c**. Assuming that the plasma is in thermal equilibrium, the Maxwell-Boltzmann distribution of the plasma is given by

$$f = n_\infty \left(\frac{\beta}{\pi}\right)^{3/2} e^{-\beta(c_1^2+c_2^2+c_3^2)} \tag{7}$$

where n_∞ is the electron density in absence of a probe, $\beta=m_e/(2kT_e)$ and c_i is the i-th component of the thermal (random) velocity. The current flux to the probe is then given by

$$J_p = e\int_{-\infty}^{\infty} dv_1 \int_{-\infty}^{\infty} dv_2 \int_{v_{3,\min}}^{\infty} v_3 f(\mathbf{v}) dv_3 = en_\infty \sqrt{\frac{\beta}{\pi}} \int_{v_{3,\min}}^{\infty} v_3 e^{-\beta c_3^2} dv_3 \tag{8}$$

where v_i is the i-th component of the total velocity and v_3 is the velocity component perpendicular to the probe. The minimum velocity, $v_{3,min}$, an electron can have and still be collected by the probe in the retarding region is given by:

$$v_{3,\min} = \left[\frac{-2e(V_p-\phi_p)}{m_e}\right]^{1/2} \tag{9}$$

Substituting a change of variable in Eq. 8 (v=c+u) and evaluating the integral over c_3, the current flux to the probe in the retarding region is given by:

$$J_p = \frac{1}{4} en_\infty \bar{v}_e \left\{ e^{-(\sqrt{V_0}-s_3)^2} + \sqrt{\pi} s_3 \left[1 - erf(\sqrt{V_0} - s_3)\right]\right\} \tag{10}$$

where $\bar{v}_e$ is the average electron velocity given by $\sqrt{8kT_e/\pi m_e}$, $V_0 = -e(V_p-\phi_p)/kT_e$ and $s_3 = \sqrt{\beta}u_3 = v_f/v_{th}$. This result takes on a form similar to classical Langmuir probe theory[18] with a correction factor added to account for the directed flow of electrons. This can be used as a fit in the retarding region of and I-V probe characteristic in order to determine electron density and electron temperature.

B. Measuring mobility

The cross-field mobility was evaluated experimentally by combining the probe measurements with the axial (anode) current. The transverse mobility, μ_{ez}, is related to the electron density, n_e, the axial current flux, J_{ez}, and the axial E-field, E_z, by $J_{ez}=qn_e\mu_{ez}E_z$. Because we know the axial field at every point in the trap we need only measure the anode current density, J_{ez}, and the electron density, n_e, in order to experimentally quantify mobility. We compute J_{ez} by measuring the anode current and surface area. Electron density is derived using the probe theory of Section IV.A. to interpret the measured probe current. Since the electric potential is known from the numerical solution of the vacuum electrostatic configuration and the electron density is low enough that the field can be assumed rigid, the probe may be biased to the known local potential as to not perturb the plasma. Combining Eq. 10 with the anode current density measurement and rearranging, mobility can be described by

$$\mu_{ez} = \frac{J_{ez}\bar{v}_e}{4J_p(V_p=\phi_p)E_z}\left\{ e^{-s_3^2} + \sqrt{\pi} s_3 \left[1 + erf(s_3)\right]\right\} \tag{11}$$

when the probe is biased to local potential where $\bar{v}_e$ is the average electron velocity, and $s_3 = \sqrt{\beta}u_3 = v_f/v_{th}$. The only unknown in Eq. 11 is electron temperature since all electric and magnetic field conditions are known and can be used to determine v_f and thus s_3. Electron temperature can be determined from a curve fit to the I-V probe

characteristic as described in Section IV.A., which can be used to determine both $\bar{v}_e$ and v_{th}. From this, mobility can be determined experimentally and then compared quantitatively with the classical model.

V. Device Performance and Discussion

A. Probe Traces

Characteristic I-V probe traces for various electric fields with the magnetic field held constant are shown in Fig. 8. The probe is positioned on channel centerline, 10 mm from the anode (at location r=160 mm and z=-45 mm in Fig. 2), and the local unperturbed plasma potential at the probe is known from numerical electrostatic models of the vacuum field. Using Eq. 10 for a curve fit in the retarding region of the probe I-V characteristic we can find electron temperature and electron density; curve fits are also shown as solid lines in Fig. 8. For the cases shown, an electron temperature of 23 eV with an electron density of $2x10^9$ m^{-3} was found for the electric field of $5.0x10^3$ V/m (corresponding to an anode-to-cathode voltage of V_{ac}=150 V), for $6.6x10^3$ V/m (V_{ac} = 200 V) electron temperature was 27 eV and density was $1.02x10^{10}$ m^{-3}, and for $8.3x10^3$ V/m (V_{ac} = 250 V), electron temperature was 58 eV and density $1.5x10^{10}$ m^{-3}. Error bars are shown to indicate uncertainty in local plasma potential due to inaccuracy in probe positioning relative to the known vacuum potential structure.

Electron temperatures measured by the probe have been found to increase with electric field by a fraction of the total available energy, as shown in Fig. 9. The electron temperatures measured by the probe are realistic given the following argument. Electrons are introduced to the trap at the surface of the cathode with very low energy (negligible when compared with the amount of energy available from the electric field) as is described in Section II.B. As electrons fall through the electric field they gain energy from the electric field. Based on the location of the probe in the anode-to-cathode gap the maximum amount of energy an electron can have at the probe is 68 percent of the anode-to-cathode potential difference. The energy gained by electrons is directionally scattered through the collisions that cause the cross-field mobility, likely inducing an isotropic energy distribution. Since we have two degrees of freedom (Larmor gyration and radial bounce within the confinement volume) we could expect to see a maximum of half of the available energy in our electron temperature (i.e. 51 eV, 68 eV and 85 eV for our respective cases of V_{ac}=150, 200, and 250). Some of this energy is lost in collisions, both elastic and inelastic, which can account for the difference between the energy available from falling through the potential difference and the measured electron temperature. Furthermore, the percent difference between measured electron energy and the total available energy from the field goes down with increasing electric field (the measured energy is 50 percent of the total available for V_{ac} =150 V, 10 percent for V_{ac} =350 V). This is because electrons in a lower electric field will undergo more collisions (energy loss mechanism) to travel the same distance because the lower temperature electrons correspond to a smaller Larmor radius and thus smaller step length per collision. It is hypothesized that because the loss mechanism decreases with increasing electric field, the electron temperature will approach a linear relationship with electric field. The electron temperature reaches an upper bound as the Larmor radius approaches trap dimensions.

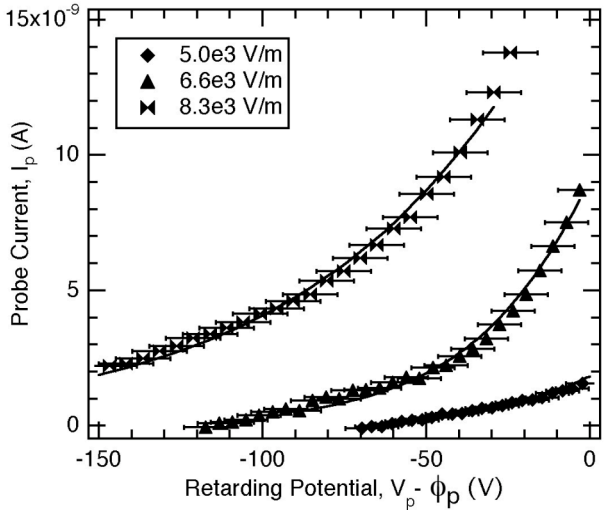

Figure 8. Current-voltage characteristics for an internal particle flux probe. Solid lines indicate best fits of the probe model given by Eq. 10.

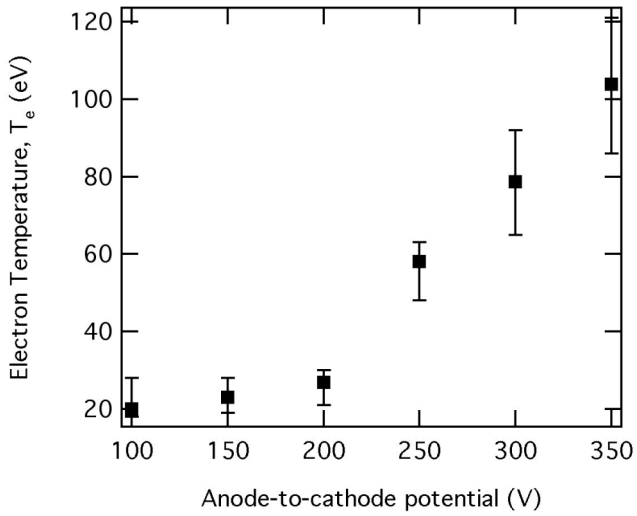

Figure 9. Electron temperature from I-V curve fits for various electric field conditions.

B. Mobility Measurements

Figure 10 shows the cross-field electron mobility versus the radial magnetic field with representative error bars for various electric fields at a constant pressure of 1.5×10^{-6} Torr, along with classical mobility and Bohm mobility. A range is indicated for classical mobility because although mobility does not depend directly on electric field, electron temperature has been found to vary with electric field. The range presented here for the fields considered corresponds to an electron temperature of 20 eV for the lowest field strength of 2.5×10^3 V/m (V_{ac} =75 V) and 97 eV for the highest field strength 1×10^4 (V_{ac} =325 V). This electron temperature was used for the determination of $\bar{v}_e$ in the equation for momentum-transfer collision frequency, $\nu_{ne} = n_0 \sigma \bar{v}_e$ and the momentum-transfer collision cross section, σ, was taken from the Siglo database[20]. As seen in the plots, the observed mobility is three orders of magnitude greater than that predicted by classical theory. Instead, the results appear to approach Bohm-like mobility, which is semi-empirically given by μ=1/(16B). Slight dependencies on electric field are apparent and could be accounted for by the variation of electron temperature with electric field. Electron temperature has been found to increase with electric field, as a greater amount of potential energy is available to the electron as it falls through the confinement volume. This change in electron temperature with electric field contributes to the measured mobility in two ways. First, it contributes to the actual mobility (which is reflected in the classical mobility as well) because a higher electron temperature corresponds to a higher electron velocity, which is directly proportional to momentum-transfer collision frequency. Second, the electron temperature affects the shape and location of the potential well of the trap. An increase in electric field will cause a proportional increase in the parallel electric field force, which is equal in magnitude at the inner and outer radii. However, the magnetic mirror force increases as $u_\perp^2$ and is stronger at the inner radius causing the potential well to shift towards larger *r*-values. This may cause the local density in the area of the probe to be lower and thus measured mobility will be higher. This may mean that measured mobility is highly sensitive to probe positioning, as the minimum of the potential well shifts radially outward with increasing electron temperature.

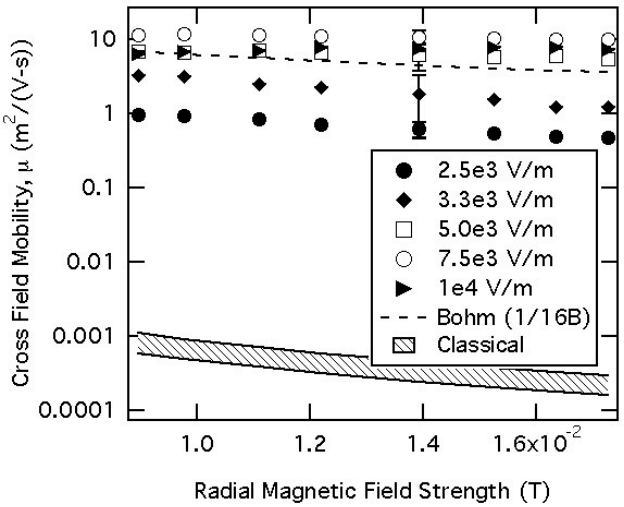

Figure 10. Cross-field mobility versus magnetic field with pressure held constant at 1.5e-6 Torr for various electric field conditions.

Figure 11 shows the cross-field electron mobility versus the radial magnetic field with representative error bars for various pressures at a constant electric field of 6.7×10^3 V/m (V_{ac}=200 V) along with classical mobility and Bohm mobility. Again, results in measured mobility are on the order of Bohm mobility rather than classical mobility. A representative case is shown in Fig. 12 where the mobility is shown versus background pressure for an electric field of 6.7×10^3 V/m (V_{ac} =200 V) and magnetic field of 152 G. Collisional classical mobility would indicate that the cross-field mobility would scale 1:1 with background pressure (i.e. neutral density, n_0), as $\mu \sim \nu_{ne}$ and $\nu_{ne} = n_0 \sigma \bar{v}_e$. Mobility increases with background pressure as is expected but a power law curve fit corresponds to a relation of $\mu \sim \nu_{ne}^{1/2}$ rather than a directly proportional relationship. These results were consistent with results obtained in previous experiments with this electron trap[21].

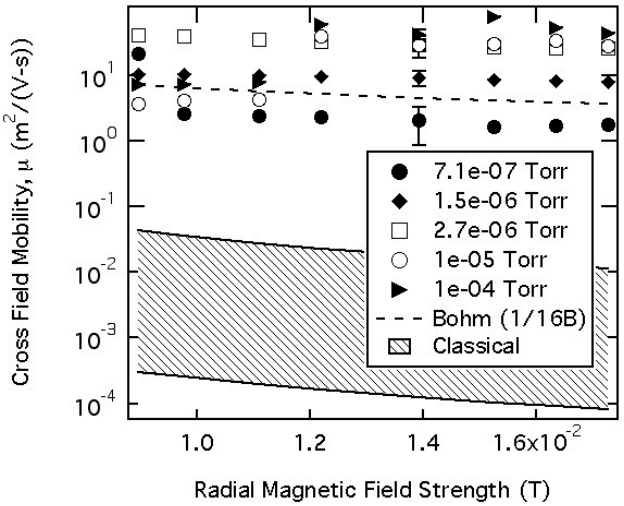

Figure 11. Cross-field mobility versus magnetic field with electric field held constant at 6.7×10^3 V/m for various pressure conditions.

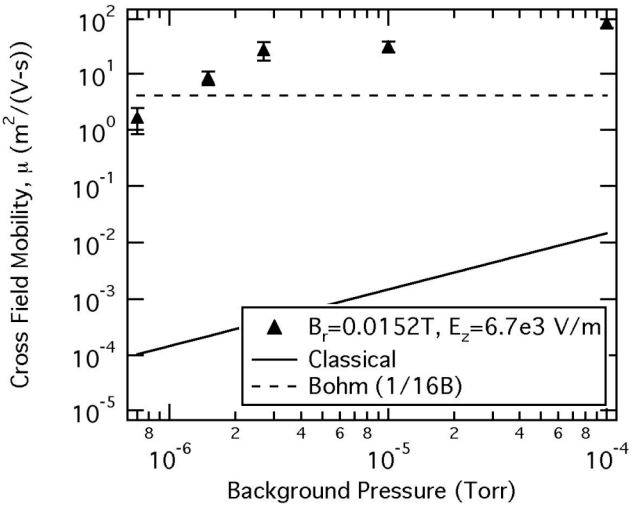

Figure 12. Cross-field mobility versus magnetic field with electric field held constant at 6.7×10^3 V/m for various pressure conditions.

VI. Conclusion

Concepts have been explored for examining a non-neutral plasma in order to study mobility, which is relatively new to Hall thruster research. This paper presents a description of an apparatus that can be used to investigate electron mobility in Hall thruster fields absent from quasi-neutral plasma effects and wall effects. The approach presented here decouples the cross-field mobility from complicating ion effects and wall effects by conducting measurements on a pure electron plasma in a highly controlled environment. This ability to decouple electron motion from plasma effects and control the electric field externally gives rise to a wealth of experiments involving optimized magnetic fields or externally applied electrostatic perturbations. The first stage of this research was to measure mobility in simplified fields and validate it against the classical mobility model. Cross-field mobility was observed that was up to three and four orders of magnitude higher than the classical prediction. Rather, the measured mobility is on the same order of Bohm-like mobility. Sensitivity to probe position may account for some discrepancy in the measured mobility but it is highly unlikely that probe positioning can account for three to four orders of magnitude differences. Therefore, it is apparent that classical mobility was not observed in this investigation.

Future work will focus on measurements of electron density and electron temperature over the entire confining volume cross-section. Density has been assumed to be constant radially and axially within the trap volume and an average mobility over the trap cross section has been assumed. If electron velocity is assumed to be isotropic the potential well created by the magnetic bottle will be uniformly filled, as the mirror reflection point does not depend on temperature but only depends on the angle of the velocity vector with respect to the magnetic field lines. However, if this assumption does not hold, the probe measurements, particularly of density, will be sensitive to radial position. Probe measurements will be taken at various radial positions within the confining volume to determine the electron density gradients along field lines. Additionally, the electron temperature measurements allude to the fact that electron temperature varies with axial position within the trap. Probe measurements will also be taken at various axial locations to determine axial gradients of electron temperature, which would correspond to an axially varying mobility.

References

[1] Chen, F. F., *Introduction to Plasma Physics and Controlled Fusion*, 2nd ed., Plenum Press, New York, 1984.

[2] Janes, G.S., and Lowder, R.S., "Anomalous Electron Diffusion and Ion Acceleration in a Low-Density Plasma," *Physics of Fluids*, **Vol. 9**, No. 6, (1966), pp. 1115-1123.

[3] Meezan, N.B., Hargus, W.A. Jr., and Cappelli, M.A., "Anomalous Electron Mobility in a Coaxial Hall Discharge Plasma," *Physical Review E.*, **Vol. 63**, No. 2, (2001) pp. 026410-1-7

[4] G. Guerrini and C. Michaut, "Characterization of high frequency oscillations in a small Hall-type thruster," *Physics of Plasmas,* **Vol. 6**, (1999) pp. 343.

[5] J.P. Boeuf and L. Garrigues, "Low Frequency Oscillations in a Stationary Plasma Thruster," *Journal of Applied Physics*, **Vol. 84**, pp. 3541.

[6] deGrassie, J.S., and Malmberg, J.H., "Waves and transport in the pure electron plasma," *Physics of Fluids*, **Vol. 23**, 63 (1980).

[7] M. Keidar et al, "Plasma flow and plasma-wall transition in Hall Thruster Channel," *Physics of Plasmas*, **Vol. 8**, pp. 5315.

[8] King, L. B., "A (Re-)Examination of Electron Motion in Hall Thruster Fields", *29th International Electric Propulsion Conference*, IEPC-2005-258.

[9] Malmberg, J.H., Driscoll, C.F., Beck, B., Eggleston, D.L., Fajans, J., Fine, K., Huang, X.-P., and Hyatt, A.W., in Non-Neutral Plasma Physics, edited by C.W. Roberson and C.F. Driscoll, *AIP Conference Proc.* Vol. 175, No. 28, 1988.

[10] Chao, E.H., Davidson, R.C., Paul, S.F., and Morrison, K.A., "Effects of background gas pressure on the dynamics of a nonneutral electron plasma confined in a Malmberg-Penning trap," *Physics of Plasmas*, **Vol. 7**, No. 3, March 2000, pp. 831-838.

[11] Robertson, S., and Walch, B., "Electron confinement in an annular Penning trap," *Physics of Plasmas*, **Vol. 7**, No. 6, June 2000, pp. 2340-2347.

[12] Espejo, J., Quraishi, Q., and Robertson, S., "Experimental measurement of neoclassic mobility in an annular Malmberg-Penning trap," *Physical Review Letters*, **Vol. 84**, No. 24, 12 June 2000, pp. 5520-5523.

[13] Robertson, S., Espejo, J., Kline, J., Quraishi, Q, Triplett, M., and Walch, B., "Neoclassical effects in the annular Penning trap," *Physics of Plasmas*, **Vol. 8**, No. 5, May 2001, pp. 1863-1869.

[14] Pedersen, T. S., Boozer, A. H., Kremer, J.P. and Lefrancois, R., "Confinement of plasmas of arbitrary neutrality in a stellarator," *Physics of Plasmas*, **Vol. 11**, No. 5, May 2004, pp. 2377-2381.

[15] Linnell, J. A. and Gallimore, A. D., "Internal Plasma Structure Measurements Using Xenon and Krypton Propellant," *International Electric Propulsion Conference*, IEPC2005-024.

[16] http://www.ansoft.com/maxwellsv/

[17] Himura, H., Nakashima, C., Saito, H. and Yoshida, Z., "Probing of flowing electron plasmas," *Physics of Plasmas*, **Vol. 8**, No. 10, Oct. 2001, pp. 4651-4658.

[18] Kremer, J.P., Pedersen, T.S., Mrkstiner, Q., Lefrancois, R.G., and Hahn, M., "Diagnosing pure-electron plasmas with internal particle flux probes," *Review of Scientific Instruments*, **Vol. 78**, No. 013503, Jan. 2007

[19] Gombosi, T. I., *Gaskinetic Theory*, Cambridge University Press, New York, NY, 1994

[20] The Siglo Data base, CPAT and Kinema Software, http://www.siglo-kinema.com

[21] Fossum, E. C., King, L. B., and Makela, J. M. "Mobility Studies of a Pure Electron Plasma in Hall Thruster Fields,"*42nd AIAA/ASME/SAE/ASEE Joint Propulsion Conference & Exhibit,* 9-12 July 2006, Sacramento, California.